Reflection Properties of Coupled-Ring Reflectors

Youngchul Chung, *Member, IEEE*, Doo-Gun Kim, and Nadir Dagli, *Senior Member, IEEE*

***Abstract*—The reflection properties of a coupled-ring reflector (CRR) are analyzed using the transfer matrix method. The CRR is composed of two coupled rings that are coupled to a bus waveguide. Depending on the combination of the cross-coupling ratios of the couplers, the reflection spectrum shape changes greatly. In the lossless case, the reflection spectrum has four peaks when the ring–bus coupling ratio is small. When the ring–bus coupling ratio is more than half and the ring–ring coupling is very small, the four peaks broaden, forming a single peak with still considerably narrow reflection spectrum, which makes the CRR attractive in applications requiring compact reflectors such as for single-mode laser diodes. The dependence of the propagation and insertion losses of the couplers on the reflection spectrum is also investigated, and the design guidelines are presented.**

***Index Terms*—Integrated optics, ring resonators, tunable filters.**

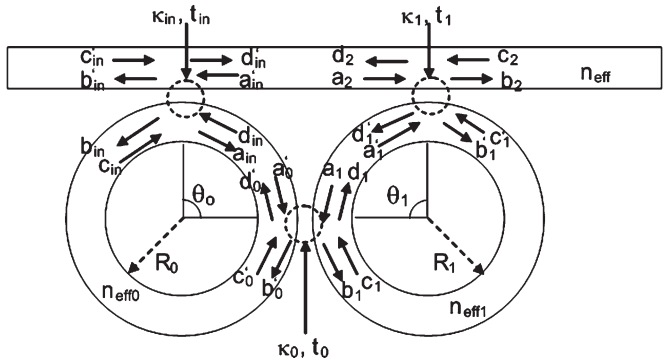

Fig. 1. Schematic configuration of CRR.

I. Introduction

THE CONCEPT of photonic integrated circuits (PICs) has been widely used to realize functional devices for dense wavelength-division multiplexing (DWDM) systems or optical signal processing systems. An arrayed waveguide grating (AWG) that is fabricated in silica or InP materials is one of the representative PIC devices [1]–[4]. Other commonly used PICs are multiwavelength laser diodes or tunable laser diodes for DWDM systems, in which the AWG or the distributed Bragg reflector (DBR) is integrated with an active medium, or the laser diodes integrated with electroabsorption modulators, Mach–Zehnder modulators, or optical amplifiers. These devices have been extensively developed and commercialized [5], [6]. Despite the successful developments of such PICs, the scale of integration is still small, and several approaches have been pursued for the large-scale integration. Microring resonators are good candidates for the building block in the large-scale integration of PICs [7]–[15].

Ring resonators are wavelength-selective devices and could be used for DWDM wavelength filters [7]–[12]. The critical coupling property of the ring resonators can also be used to build narrowband modulators or wavelength-dependent switches that can be controlled with a small amount of voltage or optical intensity [13], [14]. Furthermore, the microring resonator, coupled with crossing waveguides, can be used to change the propagation direction of the optical wave at very large angles at the resonant wavelength [7]. Such large functionality, combined with compact size, makes possible a variety of large-scale functional PICs by laying out the properly designed microring resonators in a large scale. Most ring resonators developed up until now are in general transmission-type wavelength-selective devices. There have been several efforts to realize reflection-type microring resonators. A coupled-ring reflector (CRR) composed of odd number (> 3) of ring resonators coupled with each other has been proposed [12]. There was a report on a reflection-type ring resonator with a notch in the single ring resonator [16]. Another type of ring resonator reflector composed of Mach–Zehnder modulator and ring resonators has also been reported [17]. Recently, a CRR composed of a bus waveguide and two coupled-ring resonators, both of which are coupled to the bus waveguide, is also proposed [18]–[20]. These arrangements could be a substitute for a DBR for single-longitudinal-mode laser diodes or act as a reflective wavelength filter in a DWDM system. Furthermore, the inherent reflection property makes it possible to integrate the functional components such as modulators and switches. The tunable CRR section can be fabricated by using a conventional buried heterostructure technology and can be integrated with the gain sections by employing offset quantum well techniques, which is a simple fabrication process because of the absence of a DBR structure. Recently, a semiconductor tunable laser composed of a wavelength-selective CRR has been experimentally demonstrated [20].

In this paper, the reflection properties and design guidelines of the CRR recently proposed [18]–[20] are discussed. The schematic configuration of the CRR is shown in Fig. 1, which requires two coupled rings and a coupled bus waveguide. In this device, the clockwise wave in ring 0 is coupled to a counterclockwise wave in ring 1 that is, in turn, coupled to a backward wave in the bus waveguide. There are multiple paths through

Manuscript received June 3, 2005; revised November 15, 2005. This work was supported in part by a research grant from Kwangwoon University in 2005.

Y. Chung is with the Department of Electronics and Communications Engineering, Kwangwoon University, Seoul 139-701, Korea (e-mail: ychung@daisy.kw.ac.kr).

D.-G. Kim is with the School of Electronics and Electrical Engineering, Chung-Ang University, Seoul 156-756, Korea (e-mail: emblemdo@kist.re.kr).

N. Dagli is with the Department of Electrical and Computer Engineering, University of California, Santa Barbara, CA 93106 USA (e-mail: dagli@ece.ucsb.edu).

Digital Object Identifier 10.1109/JLT.2006.871021

which the input wave is coupled to the backward wave in the straight waveguide. Because the CRR requires only two rings, it would consume less wafer space than that proposed in [12], where at least three rings are needed. The CRR discussed in this paper could be more tolerant to fabrication errors as compared with the other types of CRRs [16], [17]. The notched CRR requires a very shallow notch that is about 20–30 nm, which may be difficult to obtain repeatedly [16]. The Mach–Zehnder-type CRR requires balanced power splitting to produce good reflection properties. In this paper, the reflection properties of the new CRR [18]–[20] are investigated in detail for various values of coupling parameters such as coupling ratios and insertion losses. In Section II, a new CRR reflector is described, and the formulation of the transfer matrix analysis is presented. In the next section, the analysis results of the CRR composed of rings with identical radii are presented. In Section IV, the wide tuning characteristics of the CRR composed of rings with slightly different radii are discussed. Finally, conclusions are drawn.

II. Transfer Matrix Analysis of CRR

The CRR composed of two coupled rings and a straight waveguide coupled with both rings are shown in Fig. 1. For the analysis of the CRR, the transfer matrix formalism [12], [15] is used. The field components in the ring are expressed as

$$\mathbf{x}_i = [\, a_i \quad b_i \quad c_i \quad d_i \,]^T \tag{1a}$$

and

$$\mathbf{x}'_i = [\, a'_i \quad b'_i \quad c'_i \quad d'_i \,]^T \tag{1b}$$

where a_i, b_i, c'_i, and d'_i are the counterclockwise propagating fields, and a'_i, b'_i, c_i, and d_i are the clockwise propagating fields in the ith ring.

The coupling from the primed field components in the ith ring to the unprimed components in the $(i+1)$th ring can be represented by

$$\mathbf{x}_{i+1} = \mathbf{P}_i \mathbf{x}'_i \tag{2}$$

where the coupling matrix $\mathbf{P}_i$ is given by

$$\mathbf{P}_i = \frac{1}{-i\kappa_i} \begin{bmatrix} -t_i & 1 & 0 & 0 \\ -T_i & t_i^* & 0 & 0 \\ 0 & 0 & -t_i & 1 \\ 0 & 0 & -T_i & t_i^* \end{bmatrix}. \tag{3}$$

In the preceding equation, κ_i and t_i are the cross-coupling field ratio and the straight-through ratio, respectively, of the coupler i $(i = in, 0, 1)$, and $T_i = |\kappa_i|^2 + |t_i|^2$ is the power transmission of the coupler i. Then, the relationships between the primed fields can be expressed as

$$\mathbf{x}'_0 = \mathbf{Q}_0 \mathbf{x}_{in} = \mathbf{Q}_0 \mathbf{P}_{in} \mathbf{x}'_{in} \tag{4}$$

and

$$\mathbf{x}'_1 = \mathbf{Q}_1 \mathbf{x}_1 = \mathbf{Q}_1 \mathbf{P}_0 \mathbf{x}'_0 \tag{5}$$

where

$$\mathbf{Q}_i = \begin{bmatrix} 0 & 0 & 0 & e^{-j\beta_i R_i \theta_i} \\ 0 & 0 & e^{j\beta_i R_i (2\pi - \theta_i)} & 0 \\ & e^{-j\beta_i R_i \theta_i} & 0 & 0 \\ e^{j\beta_i R_i (2\pi - \theta_i)} & & 0 & 0 \end{bmatrix}. \tag{6}$$

Finally, we obtain

$$\mathbf{x}_2 = \mathbf{P}_1 \mathbf{Q}_1 \mathbf{P}_0 \mathbf{Q}_0 \mathbf{P}_{in} \mathbf{x}'_{in} = \mathbf{B} \mathbf{x}'_{in}. \tag{7}$$

We also have

$$a_2 = d'_{in} e^{-j\beta L} \tag{8a}$$

$$d_2 = a'_{in} e^{j\beta L} \tag{8b}$$

where L is the length of the bus waveguide between two couplers.

Assuming that $c'_{in} = 1$ and $c_2 = 0$, and combining (7) and (8), we can get

$$\begin{bmatrix} a'_{in} \\ b'_{in} \\ d'_{in} \\ b_2 \end{bmatrix} = \begin{bmatrix} B_{11} & B_{12} & B_{14} - e^{-j\beta L} & 0 \\ B_{21} & B_{22} & B_{24} & 1 \\ B_{31} & B_{32} & B_{34} & 0 \\ B_{41} - e^{j\beta L} & B_{42} & B_{44} & 0 \end{bmatrix}^{-1} \begin{bmatrix} -B_{13} \\ -B_{23} \\ -B_{33} \\ -B_{43} \end{bmatrix}. \tag{9}$$

From (9), the transmission coefficient b_2 and the reflection coefficient b'_{in} can be calculated.

III. Reflection Characteristics of CRR Composed of Rings With Identical Radii

The power reflectivity as a function of wavelength is calculated for various ring–bus coupling ratio values while the ring–ring coupling ratio is kept constant $(\kappa_0 = 0.08)$ and is shown in Fig. 2. The straight-through ratio of each coupler is given by $t_i = (T_i - |\kappa_i|^2)^{1/2}$, where $1 - T_i$ is the insertion loss of the couplers. The radii of the rings are the same and set to be 50 μm. The effective refractive indexes of all the waveguides are set to be 3.29 at $\lambda_0 = 1.55$ μm, and the group index is assumed to be 3.7. As a first-order approximation, the effective refractive index is assumed to vary linearly versus the wavelength near $\lambda_0 = 1.55$ μm. The insertion losses of the couplers are assumed to be zero in the calculation, i.e., $T_i = 1$. When the ring–bus coupling ratios (κ_{in} and κ_1) are 0.08, four reflection peaks appear in the spectrum as shown in Fig. 2(a). In the inset of Fig. 2(a), the detailed spectrum of the left double peak is shown. The reflection spectra shown in Fig. 2 are one of the repetitive spectrum shapes separated by one free spectral range (FSR). As the magnitude of the ring–bus coupling ratio increases, the four split peaks broaden and evolve into two peaks, and then finally into a single blunt peak, which is shown in Fig. 2(b) and (c). In the course of transforming into a single blunt peak, a flat-top filter response appears. That is, it is possible to design a flat-top reflection filter by adjusting the magnitudes of the coupling ratios. After a single peak is

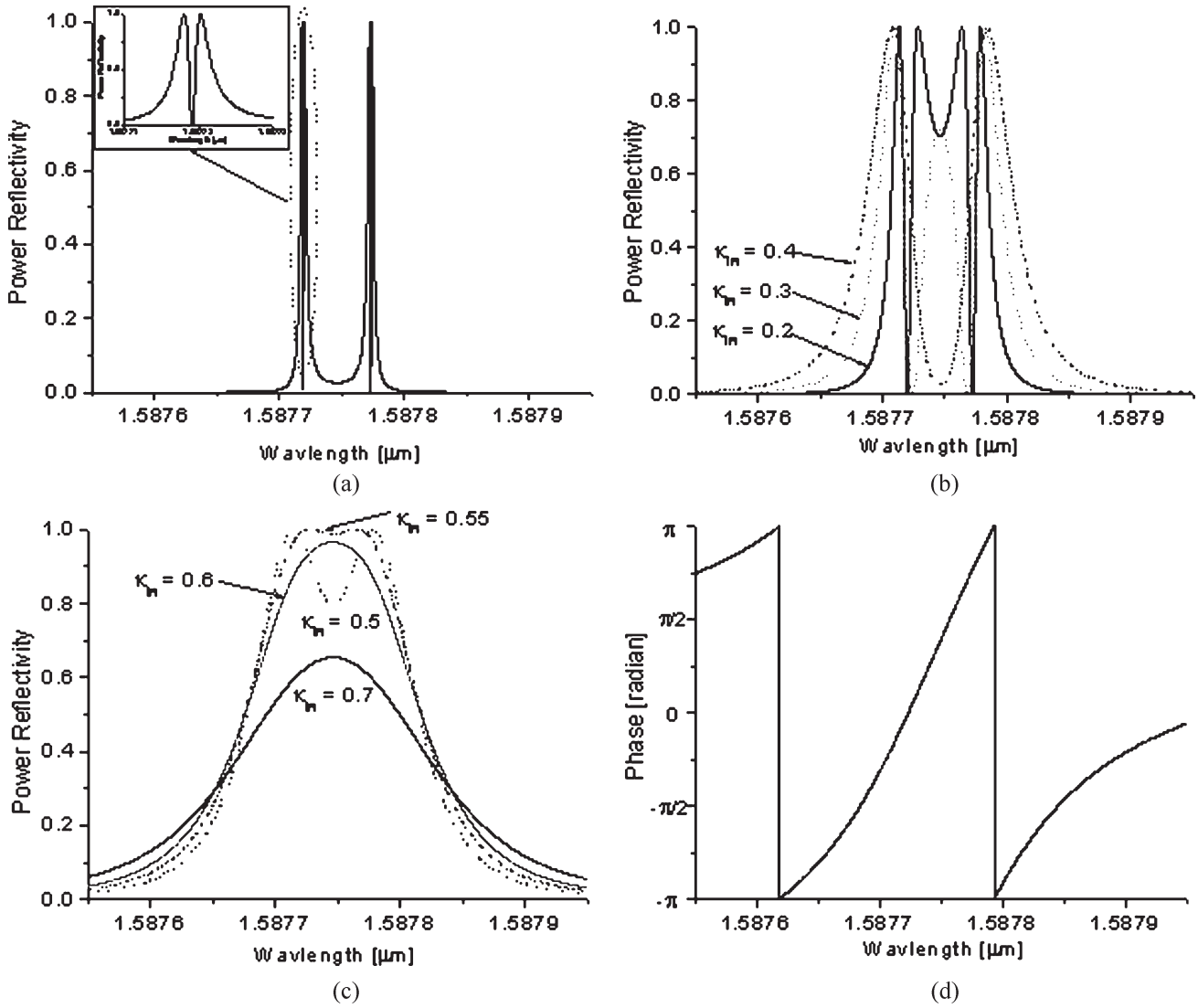

Fig. 2. Power reflectivity as a function of wavelength (a) for $\kappa_{in} = \kappa_1 = 0.08$, (b) for $\kappa_{in} = \kappa_1 = 0.2$, 0.3, and 0.4, and (c) for $\kappa_{in} = \kappa_1 = 0.5$, 0.55, 0.6, and 0.7. The ring–ring coupling ratio (κ_0) is set to 0.08. (d) Phase of reflection coefficient for $\kappa_{in} = \kappa_1 = 0.6$. In the inset of (a), the detailed reflection spectrum for the even mode is shown.

formed, the peak reflection value reduces as the magnitude of the coupling ratios further increases. With proper choices of coupling ratio values, the reflection spectrum is similar to that of the DBR, which makes it possible to apply the CRR as an integrated mirror for the tunable or fixed single-mode laser diode. In Fig. 2(d), the phase variation versus the wavelength is also shown.

We also investigate the reflection behavior of the CRR as the ring–ring coupling ratio (κ_0) changes while the ring–bus coupling ratio (κ_{in} and κ_1) is maintained to be small, which is set to 0.08. In Fig. 3(a), the reflectivity is plotted as a function of wavelength for $\kappa_0 = 0.1$, 0.707, and 1. The detailed reflectivity spectrum for each pair of peaks is almost the same as that shown in Fig. 2(a) and does not change as the ring–ring coupling ratio varies. The separation between two pairs of peaks becomes larger as the ring–ring coupling ratio increases. The separation is 0.07, 0.54, and 1.10 nm when the ring–ring coupling ratio is 0.1, 0.707, and 1, respectively. Here, the ring–bus coupling ratios are assumed to be 0.08, and $n_{\text{eff}0} = n_{\text{eff}1} = 3.29$ at the wavelength of 1.55 μm.

In order to understand the behavior of the reflection spectra, let us first consider a single isolated ring resonator of perimeter L. The resonance condition of such a ring is given by

$$\frac{2\pi}{\lambda} n_{\text{eff}}(\lambda) L = m2\pi. \tag{10}$$

The effective refractive index, which depends on the wavelength, is approximated as a linear function of wavelength over a narrow wavelength range as

$$n_{\text{eff}}(\lambda) = n_{\text{eff}}^0 + (\lambda - \lambda_0)\frac{dn_{\text{eff}}}{d\lambda} = n_{\text{g}} + \lambda\frac{dn_{\text{eff}}}{d\lambda} \tag{11}$$

where n_{g} is the group index, and n_{eff}^0 is the effective index at λ_0. Therefore, the mth-order resonance wavelength is expressed as

$$\lambda_m = \frac{L}{m} n_{\text{g}} \left[1 - \frac{L}{m}\frac{dn_{\text{eff}}}{d\lambda}\right]^{-1}. \tag{12}$$

Now, consider two coupled rings only. In this case, due to symmetry, we expect two types of resonances as schematically

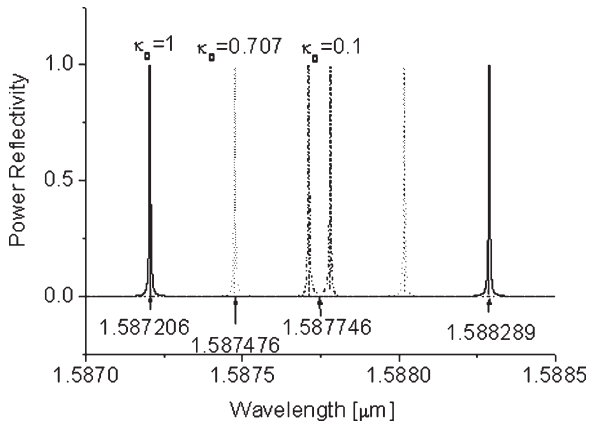

Fig. 3. (a) Power reflectivity as a function of wavelength for $\kappa_0 = 0.08$, 0.2, and 0.3. The ring–bus coupling ratios κ_{in} and κ_1 are set to 0.08. (b) Separation of peaks as a function of the ring–ring coupling ratio.

illustrated in Fig. 4. These are the so-called symmetric and antisymmetric modes. Fig. 4 illustrates the main field component and its amplitude variation at a given instant of time. In practice, the number of variations m is much higher. These field distributions rotate clockwise and counterclockwise in the left and right rings, respectively. However, the symmetric and the antisymmetric modes maintain even and odd symmetries, respectively, at all times. From this illustration, it is observed that the excitation of the coupler between the rings is symmetric for the symmetric mode and antisymmetric for the antisymmetric mode. The field amplitude distributions for these two cases are illustrated in Fig. 4. In both cases, the field amplitude distribution in the left ring remains the same, but the distributions in the right ring are 180° out of phase for the symmetric and antisymmetric modes. Therefore, to include a phase change through the coupler, the resonance condition for the symmetric and antisymmetric modes should be modified as

$$\frac{2\pi}{\lambda} n_{\text{eff}}(\lambda) L \pm \phi = m2\pi \tag{13}$$

where

$$\phi = \tan^{-1}\left(\frac{\kappa_0}{t_0}\right). \tag{14}$$

This would shift the resonance wavelength to

$$\lambda_m = \frac{L}{m \pm \frac{\phi}{2\pi}} n_{\text{g}} \left[1 - \frac{L}{m \pm \frac{\phi}{2\pi}} \frac{dn_{\text{eff}}}{d\lambda}\right]^{-1}. \tag{15}$$

Therefore, the resonance wavelength of an isolated ring splits into two when there are two coupled rings. The splitting increases as the degree of coupling between the rings increases. In the presence of the bus coupled to both rings, the presence of coupling further splits the symmetric and antisymmetric modes. The degree of this splitting depends on the strength of the ring–bus coupling ratio.

We can compare the numerical calculation presented in Fig. 3 with the predictions of this argument. Using the same numbers and (12), the resonance wavelength of a single ring for $m = 649$ is calculated to be 1.587746 μm. This is the same as the midpoints of the spectra shown in Fig. 3(a). The resonances above and below the midpoint correspond to the symmetric and antisymmetric modes that split due to coupling to the bus. Separation between the centers of split symmetric and antisymmetric modes increases as the strength of the ring–ring coupling increases. In this case, the coupling to the bus is very weak; hence, we have approximately two isolated rings. Therefore, the center of each split mode can be predicted using (15). If we do this calculation for $\kappa_0 = 0.1$, 0.707, and 1, we obtain the center wavelengths for the symmetric mode as 1.587712, 1.587476, and 1.587206 μm, respectively. These values are almost exactly the same as those calculated from the transfer matrix method. Therefore, the presence of the symmetric and antisymmetric modes is due to ring–ring coupling. The strength of this coupling controls the separation of these two modes. Further splitting of these modes is due to coupling to the bus. The separation of this splitting and its broadening is controlled by the degree of the ring–bus coupling. This argument shows that in order to get a narrow reflection spectrum, ring–ring coupling should be very low, resulting in a very small separation between the symmetric and antisymmetric modes. Then, to convert the entire reflection spectrum into a single one, the ring–bus coupling should be increased to broaden the individual splitting of the symmetric and antisymmetric modes. If done properly, it is possible to obtain a strong reflection over a narrow wavelength range.

To investigate the broadening of each reflection peaks versus the ring–bus coupling ratio (κ_{in} and κ_1), the reflection spectra are calculated, assuming the ring–ring coupling ratio (κ_0) is fixed to be 1. In this case, the reflection spectra repeat themselves with a period of half an FSR of an isolated ring. Therefore, the variation of the peaks in terms of the ring–bus coupling ratio can be observed in detail. The 3-dB bandwidth of each peak is plotted as a function of the ring–bus coupling ratio in Fig. 5. As the ring–bus coupling ratio increases to 0.6, the width of the peak broadens to 0.17 nm, which is comparable to the 3-dB bandwidth of the reflection spectrum shown in Fig. 2(c).

Flat-top reflection spectra can be obtained with an appropriate pair of ring–ring and ring–bus coupling ratios. Several reflection spectra with flat-top response are calculated using (9) and shown in Fig. 6(a). The 3-dB bandwidth as a function of the ring–ring coupling ratio is plotted in Fig. 6(b). The bandwidth increases to 0.17 nm as the ring–ring coupling ratio increases to 0.1. The 3-dB bandwidth is about 2.5 times the splitting of the pairs of peaks, which is illustrated in Fig. 3. The ring–bus coupling ratio to ensure flat-top response is also shown in Fig. 6(b). Given the ring–ring coupling ratio, the ring–bus coupling ratio for the flat-top reflection spectrum can be found. Then, the 3-dB width of the broadened peaks corresponding to the ring–bus coupling ratio shown in Fig. 5 is found to be almost the same as the 3-dB bandwidth of the reflection spectrum shown in Fig. 6. In other words, the 3-dB bandwidth is determined from the broadening of the peaks with increasing values of the ring–bus coupling. The peak value of the reflection becomes smaller than unity if we adopt the ring–bus coupling ratio corresponding to the values above the ring–bus coupling curve shown in Fig. 6(b).

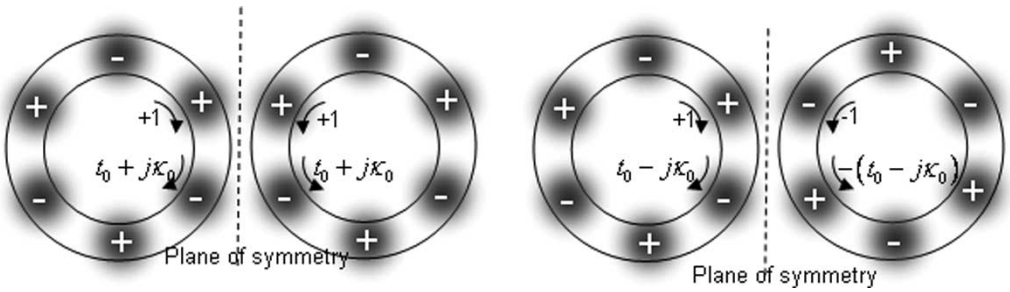

Fig. 4. Schematic illustration of symmetric and antisymmetric modes of two coupled rings.

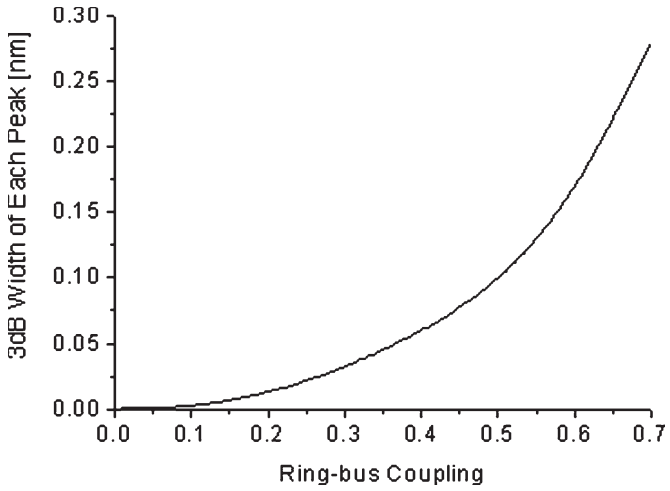

Fig. 5. Three-db width of each reflection peak as a function of ring–bus coupling ratio ($\kappa_{in} = \kappa_1$). $\kappa_0 = 1$.

A simple reflectivity formula can be derived from (9) when the ring–bus coupling ratios are the same ($\kappa_{in} = \kappa_1$), the ring radii are the same ($R_1 = R_2$), and the waveguides and couplers are lossless. The power reflectivity is given as

$$R(\lambda) = \frac{4\rho^2(\cos\,\phi - \cos\,\phi_0)^2}{[(\cos\,\phi - \cos\,\phi_0)^2 + \rho^2]^2} \tag{16}$$

where $\phi = (2\pi/\lambda)n_{\text{eff}}2\pi R_1$, $\cos\,\phi_0 = (t_0/2t_1)(1+t_1)^2$, and $\rho = \kappa_0\kappa_1^2/2t_1$. The condition for the single-peak (flat-top) spectrum is especially important for the application to reflective filters and is given by

$$\kappa_1 = \frac{\sqrt{2\kappa_0^2 + 2\sqrt{2}\kappa_0 + 2\kappa_0\sqrt{1-\kappa_0^2}}}{1+\sqrt{2}\kappa_0}. \tag{17}$$

The same formula has been derived independently by other research groups, and the conditions for various reflection spectrum shapes have been presented recently [21].

In many cases, the insertion loss of the couplers cannot be ignored. The reflection spectra for the insertion loss of 10%, 5%, 1%, and 0% ($T = 0.9$, 0.95, 0.99, and 1) are shown in Fig. 7. In Fig. 7(a), the coupling ratios of all the couplers are assumed to be 0.08. In this case, the peak reflectivity degrades very rapidly as the insertion loss of the couplers increases. Furthermore, four sharp peaks broaden and become a single blunt peak. When $T = 0.95$, the peak reflectivity substantially decreases to 0.012. In Fig. 7(b), the ring–bus coupling ratios

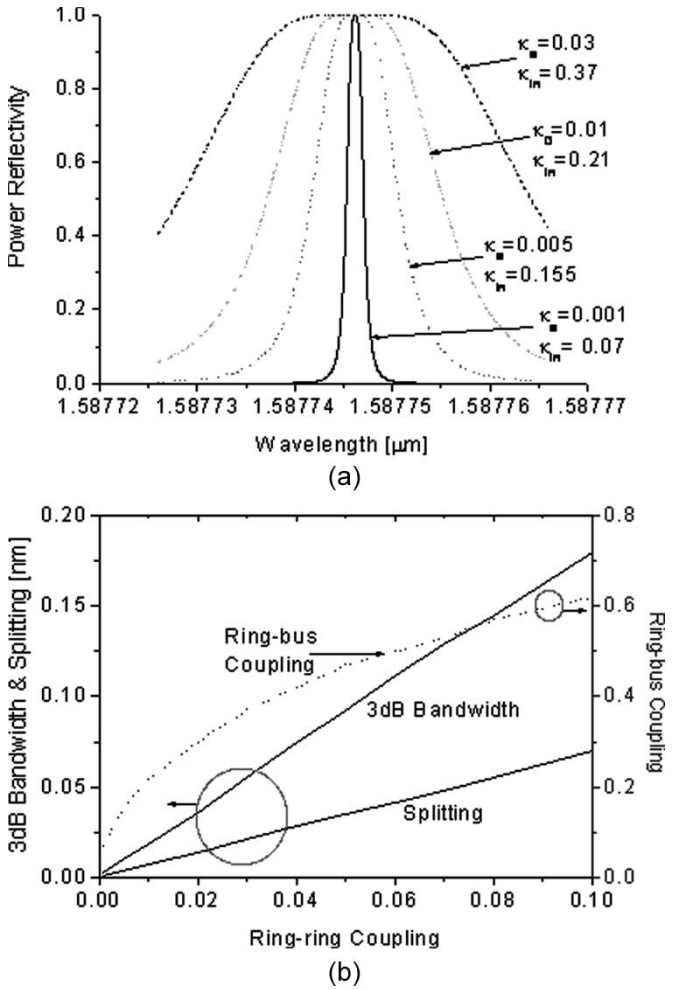

Fig. 6. (a) Several reflection spectra with flat-top response. Appropriate pairs of ring–ring coupling ratio (κ_0) and ring–bus coupling ratio ($\kappa_{in} = \kappa_1$) should be selected to exhibit flat-top response. (b) Three-db bandwidth of reflection spectrum with flat-top response and the splitting of pairs of peaks as a function of ring–ring coupling. The ring–bus coupling values to ensure flat-top responses are also plotted with dotted line.

are assumed to be 0.6, and the ring–ring coupling ratio is 0.08. Compared with Fig. 7(a), the peak reflectivity degrades slowly as the insertion loss increases. When $T = 0.95$, the peak reflectivity is about 0.2. In Fig. 7(c), the coupling ratios of the input and output couplers are assumed to be 0.7, and that of the coupler between rings is 0.08. When $T = 1$, the peak reflectivity is about 0.655. When T is reduced to 0.95, the peak reflectivity is decreased to about 0.312, which is larger than in the case of $\kappa_{in} = \kappa_1 = 0.6$. In Fig. 7, it is observed that the

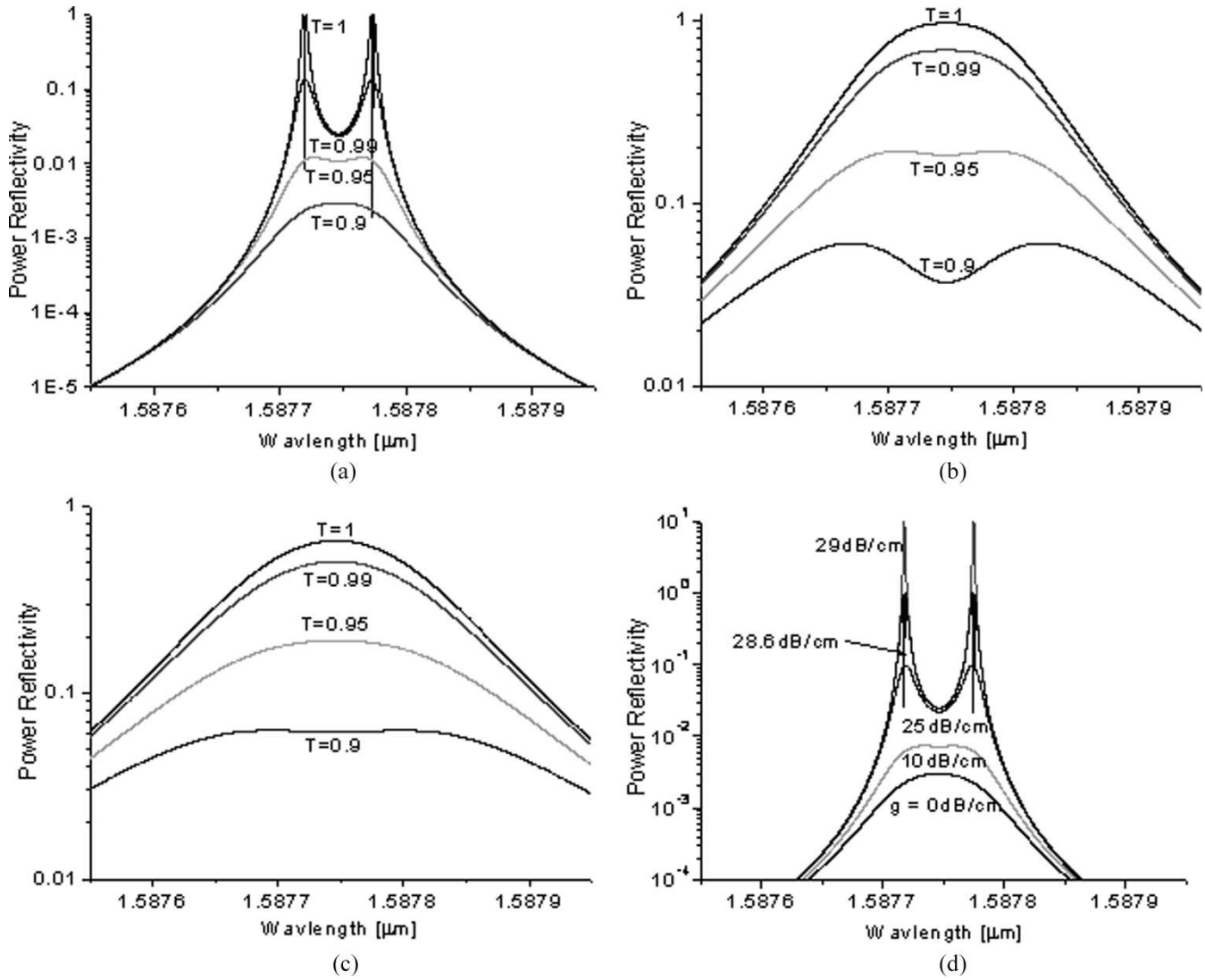

Fig. 7. Power reflectivity as a function of wavelength for $T = 0.9, 0.95, 0.99$, and 1. (a) κ_{in}, κ_1, and κ_0 are all assumed to be 0.08. (b) κ_{in} and κ_1 are assumed to be 0.6, and κ_0 is 0.08. (c) κ_{in} and κ_1 are assumed to be 0.7, and κ_0 is 0.08. (d) Power reflectivity as a function of wavelength for $T = 0.9$. κ_{in}, κ_1, and κ_0 are all assumed to be 0.08. Several gain values in the ring waveguides are assumed.

degradation of the peak reflectivity value with the insertion loss increase is less sensitive as the magnitude of coupling ratios κ_{in} and κ_1 increases. The degradation of the reflectivity due to the insertion loss of the coupler could be compensated by introducing the gain in the ring waveguides. In Fig. 7(d), the reflectivities for $T = 0.9$ are plotted for various values of gain coefficient while the coupling ratios of all the couplers are assumed to be 0.08. When the gain in the ring waveguides is 28.6 dB/cm, the insertion loss of the couplers can be fully compensated and the lossless response, as shown in Fig. 7(a), is obtained. When the loss is overcompensated, the CRR starts to show reflectivity greater than 1. In Fig. 7(d), the reflection spectrum for the gain of 29 dB/cm is also illustrated.

IV. Wide Tuning of CRR Composed of Rings With Slightly Different Radii

If the radii of the two rings in the CRR are slightly different, the resonance wavelengths of the two rings are misaligned at all the resonance wavelengths, except at certain wavelengths. By changing the refractive index of one ring in the CRR while maintaining that of the other, the peak reflection wavelength can be discretely selected by aligning the certain resonance wavelengths of two rings. It is also possible to get continuous tuning by properly changing the refractive indexes of two rings simultaneously.

The tuning range is determined by the amount of mismatch between the FSRs of the two rings and is, thus, approximately given by

$$\Delta\lambda_{\text{tune}} = \frac{\lambda_o^2}{2\pi n_{\text{g}}(R_1 - R_0)} = F\Delta\lambda_0 \tag{18}$$

where $\Delta\lambda_0$ is an FSR for ring 0, and F is a tuning enhancement factor, which is given by

$$F = \frac{R_1}{(R_1 - R_0)}. \tag{19}$$

When the radii of the rings in the CRR are $R_0 = 50$ μm and $R_1 = 52$ μm, corresponding to $F = 26$, the center wavelength

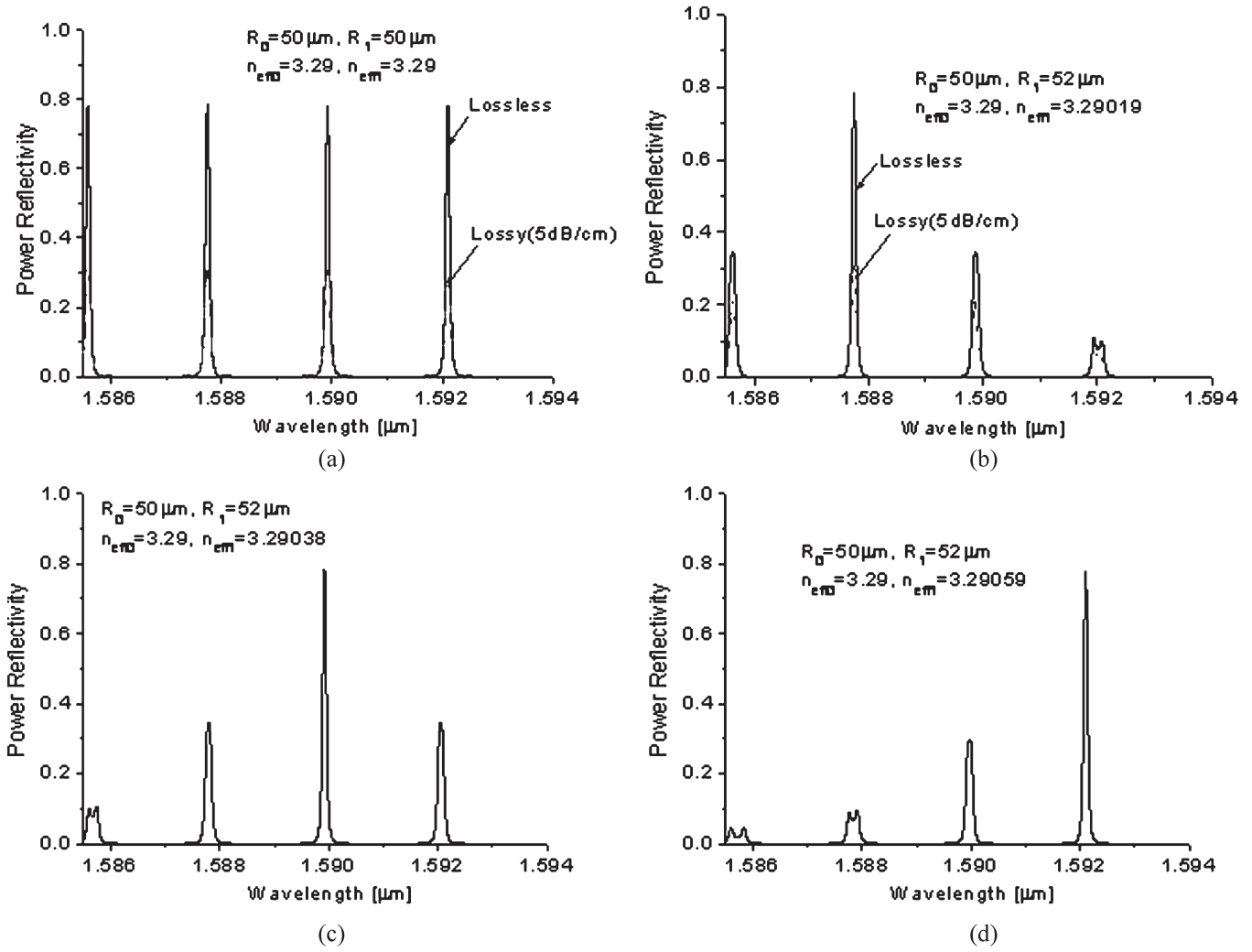

Fig. 8. Power reflectivity as a function of wavelength (a) for $n_{\text{eff}0} = n_{\text{eff}1} = 3.29$ at $\lambda = 1.55$ μm and $R_0 = R_1 = 50$ μm. Power reflectivities in case of different ring radii ($R_0 = 50$ μm and $R_1 = 52$ μm) (b) for $n_{\text{eff}1} = 3.29019$, (c) for $n_{\text{eff}1} = 3.29038$, and (d) for $n_{\text{eff}1} = 3.29059$ while $n_{\text{eff}0}$ is kept constant ($n_{\text{eff}0} = 3.29$). κ_{in} and κ_1 are assumed to be 0.5, and κ_0 is 0.04.

is 1.55 μm, the group refractive index (n_{g}) is 3.7, and the tuning range could be as wide as 52 nm.

In Fig. 8, the power reflectivities as functions of wavelength are shown for the different refractive indexes of ring 2. Here, the ring–bus coupling ratios (κ_{in} and κ_1) are assumed to be 0.5, and the ring–ring coupling ratio (κ_0) is 0.04. In Fig. 8(a), the reflectivity spectrum for $R_0 = R_1 = 50$ μm and $n^0_{\text{eff}0} = n^0_{\text{eff}1} = 3.29$ is shown. A periodic reflection response with an FSR of 2.17 nm is observed. The maximum reflectivity is 0.78, which is smaller than unity due to the relatively large coupling ratio between the straight waveguide and the rings. The reflectivity is expected to decrease when there is a loss in the waveguides. The reflectivity in case of a 5 dB/cm loss is shown as a dotted line in Fig. 8(a). The peak reflectivity is reduced to 0.31. In Figs. 8(b)–(d), the reflectivities in the case of different ring radii ($R_0 = 50$ μm and $R_1 = 52$ μm) are shown. By setting the refractive index of ring 1 to $n^0_{\text{eff}1} = 3.29019$, 3.29038, and 3.29057 at $\lambda = 1.55$ μm while maintaining the refractive index of ring 0 constant ($n^0_{\text{eff}0} = 3.29$), the wavelength of peak reflectivity can be selected sequentially to be 1.587746, 1.589918, and 1.5921 μm, respectively. The wavelength separation is about 2.17 nm, which is close to the FSR of ring 0. The CRR with different ring radii can be used for a tunable reflection filter in realizing widely tunable laser diodes [19].

In Section III, it is demonstrated that the shape of the power reflection spectrum is quite sensitive to the ring–bus coupling ratios for the CRR composed of rings with identical radii. For the CRR with slightly mismatched ring radii, the similar behavior is expected. In Fig. 9, the reflectivity for $n^0_{\text{eff}0} = 3.29$ and $n^0_{\text{eff}1} = 3.29019$ while both the ring–bus and ring–ring coupling ratios are assumed to be 0.08 is shown. Fig. 9(a) also shows the reflectivity over the range of four FSRs. Near the maximum reflection, the four peaks can be observed as detailed in Fig. 9(b), which is similar in Fig. 2(a). Further reflection shapes for various ring–bus coupling ratio while maintaining the ring–ring coupling ratio to be 0.08 are shown in Fig. 10. In the inset of each figure, the reflectivity over the wavelength range of two FSRs is also presented. As the ring–bus coupling ratio increases from 0.08 to 0.6, the four peaks become undistinguishable and a single peak appears similar to the case of identical ring radii as shown in Section III.

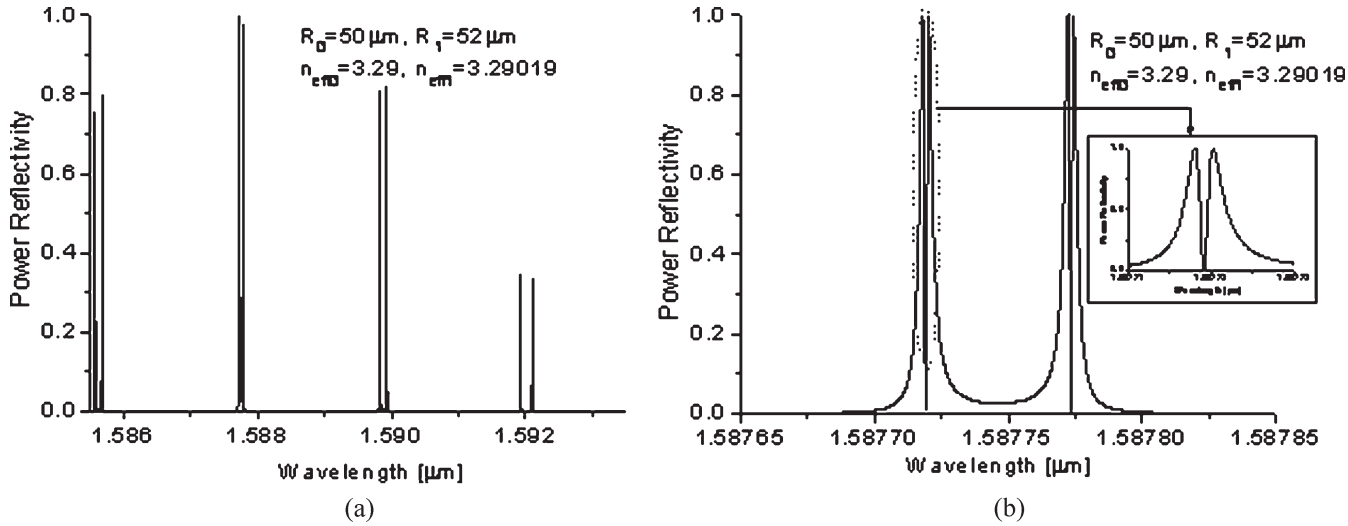

Fig. 9. (a) Power reflectivity as a function of wavelength for $n_{\text{eff}0} = 3.29$ and $n_{\text{eff}1} = 3.2898$. κ_{in} and κ_1 are assumed to be 0.08, and κ_0 is 0.08. $R_0 = 50\ \mu$m, and $R_1 = 52\ \mu$m. (b) Enlarged view of (a) in the vicinity of maximum peaks. In the inset of (b), the detailed reflection spectrum for the even mode is shown.

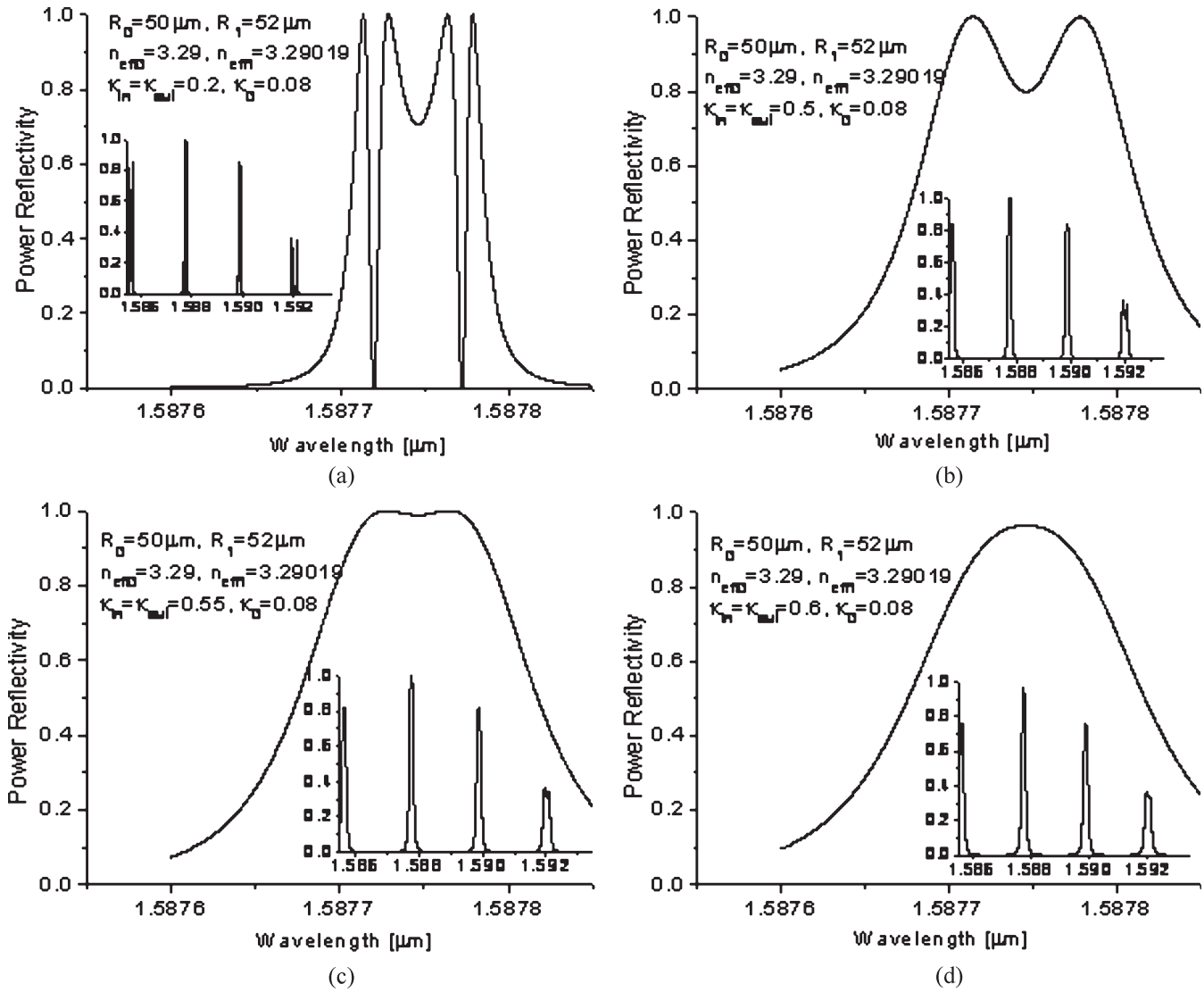

Fig. 10. Power reflectivity as a function of wavelength (a) for $\kappa_{in} = \kappa_1 = 0.2$, (b) for $\kappa_{in} = \kappa_1 = 0.5$, (c) for $\kappa_{in} = \kappa_1 = 0.55$, and (d) for $\kappa_{in} = \kappa_1 = 0.6$. The ring–ring coupling ratio (κ_0) is set to 0.08. $n_{\text{eff}0} = 3.29$, and $n_{\text{eff}1} = 3.29019$. $R_0 = 50\ \mu$m, and $R_1 = 52\ \mu$m.

V. Conclusion

Wavelength-selective reflective filters have usually been achieved through the fabrication of DBRs, and they have been used for DWDM filters or the realization of fixed or tunable laser diodes. The fabrication of DBRs requires additional holography procedures, electron-beam writing, or phase masks. Therefore, the cost-effective approach to realize wavelength-selective reflection filters simultaneously with the waveguide formation is desirable. The coupled-ring waveguide structure can be used to realize the wavelength-selective planar waveguide reflectors without resorting to DBRs.

In this paper, we analyze a new CRR that is composed of two coupled-ring waveguides and a bus waveguide coupled with both rings, and its reflection properties are presented. The characteristics of the CRR versus the cross-coupling ratios and the insertion losses of the couplers are investigated in detail. When the ring–bus coupling ratio is very small, the reflection spectrum reveals four peaks. However, as the coupling ratio becomes larger, the peaks broaden and become indistinguishable, which finally becomes a single peak with a broader spectrum. The broadened single-peak spectrum still has a quite narrow 3-dB bandwidth that is about 0.15 nm or narrower. Therefore, the CRR can be used for DWDM filters or wavelength-selective reflectors for fixed or tunable laser diodes. The splitting of resonance wavelengths due to symmetric and antisymmetric modes is identified, and it is shown that the degree of splitting becomes larger as the coupling between rings increases. To get a single narrow reflection peak, the coupling between rings should be as small as possible, and the coupling between the rings and the bus waveguide should be properly chosen. For some coupling ratio values, flat-top filter response can also be obtained. Especially, when the radii of two circular rings are slightly different from each other, a Vernier effect makes the repetition wavelength spacing of the reflection peaks greatly enhanced as compared with the FSR of the individual rings. When the ring radii are 50 and 52 μm, the peak repetition spacing is about 52 nm, which also corresponds to the tuning range of the CRR.

References

[1] J. Capmany, C. Doerr, K. Okamoto, and M. K. Smit, "Introduction to the special issue on arrayed grating routers/WDM mux/demuxs and related applications/uses," *IEEE J. Sel. Topics Quantum Electron.*, vol. 8, no. 6, pp. 1087–1089, Nov./Dec. 2002.

[2] Y. Hibino, "Recent advances in high-density and large-scale AWG multi/demultiplexers with higher index-contrast silica-based PLCs," *IEEE J. Sel. Topics Quantum Electron.*, vol. 8, no. 6, pp. 1090–1101, Nov./Dec. 2002.

[3] Y. Yoshikuni, "Semiconductor arrayed waveguide gratings for photonic integrated devices," *IEEE J. Sel. Topics Quantum Electron.*, vol. 8, no. 6, pp. 1102–1114, Nov./Dec. 2002.

[4] M. K. Smit and C. van Dam, "PHASAR-based WDM-devices: Principles, design, and applications," *IEEE J. Sel. Topics Quantum Electron.*, vol. 2, no. 2, pp. 236–250, Jan. 1996.

[5] J. S. Barton, E. J. Skogen, M. L. Mašanović, S. P. Denbaars, and L. A. Coldren, "A widely tunable high-speed transmitter using an integrated SGDBR laser-semiconductor optical amplifier and Mach–Zehnder modulator," *IEEE J. Sel. Topics Quantum Electron.*, vol. 9, no. 5, pp. 1113–1117, Sep./Oct. 2003.

[6] E. A. J. M. Bente, Y. Barbarin, J. H. Besten, M. K. Smit, and J. J. M. Binsma, "Wavelength selection in an integrated multiwavelength ring laser," *IEEE J. Quantum Electron.*, vol. 40, no. 9, pp. 1208–1216, Sep. 2004.

[7] Y. Hatakeyama, T. Hanai, S. Suzuki, and Y. Kokubun, "Loss-less multilevel crossing of busline waveguide in vertically coupled microring resonator filter," *IEEE Photon. Technol. Lett.*, vol. 16, no. 2, pp. 473–475, Feb. 2004.

[8] B. E. Little *et al.*, "Very high-order microring resonator filters for WDM applications," *IEEE Photon. Technol. Lett.*, vol. 16, no. 10, pp. 2263–2265, Oct. 2004.

[9] J. K. S. Poon, Y. Huang, G. T. Palocz, and A. Yariv, "Soft lithography replica molding of critically coupled polymer microring resonators," *IEEE Photon. Technol. Lett.*, vol. 16, no. 11, pp. 2496–2498, Nov. 2004.

[10] P. Rabiei, W. H. Steier, C. Zhang, and L. R. Dalton, "Polymer micro-ring filters and modulators," *J. Lightw. Technol.*, vol. 20, no. 11, pp. 1968–1975, Nov. 2002.

[11] P. Rabiei and W. H. Steier, "Tunable polymer double micro-ring filters," *IEEE Photon. Technol. Lett.*, vol. 15, no. 9, pp. 1255–1257, Sep. 2003.

[12] J. K. S. Poon, J. Scheuer, and A. Yariv, "Wavelength-selective reflector based on a circular array of coupled microring resonators," *IEEE Photon. Technol. Lett.*, vol. 16, no. 5, pp. 1331–1333, May 2004.

[13] A. Yariv, "Critical coupling and its control in optical waveguide-ring resonator systems," *IEEE Photon. Technol. Lett.*, vol. 14, no. 4, pp. 483–485, Apr. 2000.

[14] T. A. Ibrahim, W. Cao, Y. Kim, J. Li, J. Goldhar, P.-T. Ho, and C. H. Lee, "All-optical switching in a laterally coupled microring resonator by carrier injection," *IEEE Photon. Technol. Lett.*, vol. 15, no. 1, pp. 36–38, Jan. 2003.

[15] J. K. S. Poon, J. Scheuer, S. Mookherjea, G. T. Paloczi, Y. Huang, and A. Yariv, "Matrix analysis of microring coupled-resonator optical waveguides," *Opt. Express*, vol. 12, no. 1, pp. 90–103, Jan. 2004.

[16] B. E. Little, S. T. Chu, and H. A. Haus, "Second-order filtering and sensing with partially coupled traveling waves in a single resonator," *Opt. Lett.*, vol. 23, no. 20, pp. 1570–1572, Oct. 1998.

[17] G. T. Paloczi, J. Scheuer, and A. Yariv, "Compact microring-based wavelength-selective inline optical reflector," *IEEE Photon. Technol. Lett.*, vol. 17, no. 2, pp. 390–392, Feb. 2005.

[18] Y. Chung, D. G. Kim, and N. Dagli, "Analysis of wavelength-selective reflector composed of two coupled ring resonators," presented at the Integrated Photonics Research and Applications, San Diego, CA, Apr. 2005, Paper ITuD5.

[19] ——, "Widely tunable coupled-ring reflector laser diode," *IEEE Photon. Technol. Lett.*, vol. 17, no. 9, pp. 1773–1775, Sep. 2005.

[20] S. J. Choi, Z. Peng, Q. Yang, E. H. Hwang, and P. D. Dapkus, "A semiconductor tunable laser using a wavelength selective reflector based on ring resonators," presented at the Optical Fiber Conf., Anaheim, CA, Feb. 2005, Post-deadline Paper PDP20.

[21] I. Chremmos and N. Uzunoglu, "Reflective properties of double-ring resonator system coupled to a waveguide," *IEEE Photon. Technol. Lett.*, vol. 17, no. 10, pp. 2110–2112, Oct. 2005.

Youngchul Chung (S'89–M'92) received the B.S. degree in electronics engineering from Seoul National University, Seoul, Korea, in 1981, the M.S. degree in electrical engineering from the Korea Advanced Institute of Science and Technology, Daejon, Korea, in 1983, and the Ph.D. degree in electrical and computer engineering from the University of California, Santa Barbara (UCSB), in 1992, where he conducted research on the fabrication and modeling of photonic integrated circuit devices in III–V compound semiconductors.

From 1983 to 1986, he was a Research Engineer at LG Cable Company, Anyang, Korea, working on optical communication systems and local area network systems. Until 1988, he was a Researcher at the Korea Institute of Science and Technology, where he was involved in the analysis and fabrication of the two-mode interference wavelength-division multiplexer/demultiplexer. From 1992 to 1993, he was a Researcher at the Optoelectronics Technology Center, UCSB. Since then, he has been with the Department of Electronic and Communications Engineering, Kwangwoon University, Seoul, where he is currently a Professor. His current research interests include the design, fabrication, and modeling of passive and active guided-wave components for high-capacity optical communication systems and optical signal processing.

Dr. Chung chaired the Conference on Optoelectronics and Optical Communications (COOC 2001) in Korea.

Doo-Gun Kim received the B.S. degree in electronic engineering, the M.S. degree in image engineering, and the Ph.D degree in electronic and electrical engineering from Chung-Ang University, Seoul, Korea, in 1998, 2000, and 2003, respectively.

He is currently a Research Professor of electrical and electronic engineering at Chung-Ang University. His research interests include optical switching devices and optical biosensor devices.

Nadir Dagli (S'77–M'87–SM'04) was born in Ankara, Turkey. He received the B.S. and M.S. degrees from the Middle East Technical University, Ankara, and the Ph.D. degree from the Massachusetts Institute of Technology, Cambridge, in 1976, 1979, and 1986, respectively, all in electrical engineering.

After graduation, he joined the Department of Electrical and Computer Engineering, University of California, Santa Barbara (UCSB), where he is currently a Professor. He authored and coauthored over 100 refereed journal and conference publications. His current interests include the design, fabrication, and modeling of guided-wave components for optical integrated circuits, ultrafast electrooptic modulators, wavelength-division multiplexing components, and photonic nanostructures.

Dr. Dagli was awarded NATO science and IBM predoctoral fellowships during his graduate studies. He was the recipient of the 1990 UCSB Alumni Distinguished Teaching Award and the 1990 UC Regents Junior Faculty Fellowship. He was a member of the Editorial Board of the IEEE TRANSACTIONS ON MICROWAVE THEORY AND TECHNIQUES from 1994 to 1998. He was an Associate Editor of IEEE PHOTONICS TECHNOLOGY LETTERS (PTL) from 1997 to 2000. He is currently the Editor of PTL and an Elected Member of the IEEE Lasers and Electro-Optics Society Board of Governors. He was a Program Co-Chair of the Integrated Photonics Research Topical Meeting in 1998 and chaired the same conference in 1999. He was an Advisory Board Member of the Integrated Photonics Research Conference from 1999 to 2003. He served as a Program Co-Chair in 1998 and has been an Advisory Board Member of the International Topical Meeting on Microwave Photonics since 1999.